UBIQUITOUS GROWTH OF PALEOARCHEAN BIOFILMS RECORDED IN WHITE CHERT BANDS OF THE BUCK REEF CHERT

A Thesis

by

JONATHAN WILLIAM SNEED

Submitted to the Office of Graduate and Professional Studies of
Texas A&M University
in partial fulfillment of the requirements for the degree of

MASTER OF SCIENCE

Chair of Committee,	Michael M. Tice
Committee Members,	Thomas Olszewski
	Daniel Thornton
Head of Department,	Rick Giardino

December 2014

Major Subject: Geology

ABSTRACT

The 3.42 Ga Buck Reef Chert (Kromberg Formation, Barberton greenstone belt, South Africa) contains a geobiological record of microbial mats confined to the photic zone of anoxic Archean oceans. In order to better understand the early development of photosynthetic microbial systems, these records were surveyed at multiple scales using novel hydrofluoric etching methods, translucent slabs cut to mm-scale thickness, Raman spectroscopy, and thin section analysis. I demonstrate that mat growth in the photic zone was far more common and voluminous than previously thought. Biofilm growth and silica sedimentation dominated during mat growth, which was punctuated by the transport of large volumes of detrital carbonaceous grains. Further, cyclicity in the relative contributions of biomass and sedimentary silica in these microbialites can be demonstrated, showing that these cycles fall within a Poisson distribution that offers useful constraints in the growth processes that led to their formation.

ACKNOWLEDGEMENTS

I would like to thank my committee chair, Dr. Tice, and my committee members, Dr. Thornton and Dr. Olsziewski, for their continued support and expert counsel at every stage. Special gratitude goes to Dr. Debbie Thomas and Dr. Stella Woodard, who with Dr. Tice provided the first steps in what must become a lifetime of scientific inquiry.

Thanks also go to my colleagues in the Department of Geology and Geophysics. In a community that offers so much friendship and encouragement, any list of names will land far short of the reality, but such a list must at least include Jian Gong, Zhirui Zeng, Kimbra Quezegue, Julian Correa, and Matthew Wehner.

I owe much to Ada Palmer, Lauren Schiller, and Lindsey Nilsen, with whom I found a home and great strength of spirit. Final thanks are reserved for my parents, Loyd and Kathryn, who showed me that a person can become good. All else follows.

TABLE OF CONTENTS

Page

LIST OF FIGURES

Page

CHAPTER I

INTRODUCTION AND LITERATURE REVIEW

Astronomical modeling and the Paleoarchean geologic record imply a ~3.4 Ga global environment with a reducing atmosphere, a hotter and more active mantle, limited or absent tectonic plate formation, a faint young sun, and a significantly shorter day/night cycle. Despite these extreme conditions, Paleoarchean sediments also offer the earliest recognized history of life. In a geobiological framework, these microbialites may be understood as information-rich components of an interdependent global system, which constrain the processes that contribute to their formation and the environmental consequences of ancient biological productivity.

Known examples of Paleoarchean sedimentary rocks have experienced a minimum of upper prehnite-pumpellyite grade metamorphism. (e.g. Stevens & Moyen 2007) Furthermore, the development of fossil mats is constrained by a complex, nonlinear, and poorly understood set of geobiological factors (Grotzinger & Knoll, 1999). Paleoarchean microbialites within the Buck Reef Chert are exceptionally informative in this regard. Although the identification of well-preserved microfossils is often problematic in this chert (van Zuilen et. al., 2007), mat community features retain much of their original morphology. The microbialites preserve a range of environments within the euphotic zone (Tice 2009), allowing a broad sampling of microbial behavior under varying conditions. The present study examines these systems at multiple scales, with an emphasis on geological and biological processes that constrain environmental

interpretation. We test a depositional model in which biomass and mineral precipitates accumulate during energetically quiescent depositional periods, and are intermittently buried by the rapid deposition of detrital carbonaceous sediments.

This differs from established models of mat growth in the Buck Reef Chert. Existing process interpretations focus on mat growth within detrital carbonaceous layers (Tice & Lowe, 2004). These models describe the gradual biomediated accumulation of carbonaceous grains, interspersed with the abiological precipitation of chemically pure chert. Others have proposed that silica precipitation was hydrothermally driven (Hofmann & Bolhar, 2007). However, these interpretations must be reconsidered in light of new observations.

Standard methodologies developed under the expectation of Phanerozoic conditions have been supplemented by novel etching procedures in which HF aerosol preferentially reacts with carbon-poor cryptocrystalline areas, clarifying the underlying composition in otherwise undifferentiated chert and allowing a survey of grain distributions and sedimentary structures in black bands. Further, extensive use of translucent 'thin slabs' clarifies mesoscale gradations between chemically pure and carbonaceous chert bands.

Background

The cohesive properties of benthic microbial mats favor their preservation and subsequent discovery relative to planktonic bacteria. Eukaryotic organisms are often well-preserved, but their comparatively recent evolution represents a smaller fraction of

the geologic timescale. Accordingly, microbial lithologies (particularly biogenic stromatolites) account for the majority of known preserved fossil structures in many areas of interest (Allwood et al., 2009). In the absence of a generally accepted universal model of microbialite formation, this rich fossil record remains poorly constrained (Grotzinger & Knoll 1999, Tice et. al., 2011).

Often, these early records preserve whole communities rather than isolated cells. In such mats, morphology arises from environmental boundary conditions as well as the phenotypic expression of the organisms themselves (Grotzinger & Knoll, 1999; Hofmann, 1987; Batchelor et al., 2004). This dynamic is governed in modern analogues partly by extracellular polymeric substance (EPS), which exhibits behaviors ranging from grain capture to intercellular mobility via contact stimuli. (Tice et. al., 2011). These influences propagate from subcellular to macroscopic scales, substantially affecting fluid flows and associated sedimentary processes.

Precambrian beds interpreted as storm-influenced basin environments have been found to host a number of biogenic stromatolite and microbialite morphologies. The Carawine Dolomite, a 2.4 Ga deposit within Hammersley Basin, Australia, contains laminite sequences with a typical thickness on the order of 1 m. These laminations are generally planar or gently undulatory, with occasional small hemispheroidal stromatolites. These are frequently observed to nucleate around an initial point of locally high relief, such as imbricated pebble grains, and may grow directly upon other stromatolites to form stacked hemispheroids. More rarely, larger stromatolite mounds (up to 4.4 m width) are preserved. In contrast with the more common laminite and

hemispheroidal stromatolites, the internal laminations of these domes may display wavy or clumped patterns (Simonson 1993). The Reivilo, Gamohaan, and Monteville formations, interpreted as slope-basin deposits within the Transvaal Supergroup (2.3-2.6 Ga), preserves conophyton features of a similar scale. The fragility of these columns suggests quiet-water conditions. These are interspersed with graded, massive intraclast beds, strongly implying storm activity or turbidite deposits. Benthic cyanobacterial deposits (Beukes 1987), and occasional ripple sedimentary structures, constrain these deposits to the photic zone. These typically overlie peritidal and subtidal deposits, implying that a transgressive/regressive cycle has been recorded (Beukes 1987).

Modern biogenic stromatolites are ecologically constrained to the thermohaline extremes of Earth systems. Candidates include hypersaline lakes, sabkhas, and natural geysers, as well as similar anthropogenic environments. Storr's Lake, of San Salvador Island, the Bahamas, has a measured salinity of ~59 ppt, and shows depth-dependent variability in local carbonate stromatolite morphology. Although the lacustrine environment lacks significant tidal action, it is highly turbulent, with a photic zone in the tens of centimeters. Shallow bacterial growths (<5 cm) construct primarily flat mats, using a filamentous structure to bind detrital particles in loose sediment and increase surface tension. A micritic crust forms in these mats, which extend to deeper waters and act as an environmental substrate on which other morphologies occur, including classic accretionary stromatolites (Dupraz 2013). Guerrero Negro, on the Baja Peninsula, combines a natural sabkha environment with an anthropogenic saltern. Salinities range from a low of 130 ppt to a high of 300 ppt. The mesoscale microbial features of

Guerrero Negro are dominated by microbial mats and the microbially mediated precipitation of gypsum and other evaporites. In subaerial environments, biofilms grow just below clastic surface deposits, or are not found. In intertidal and supratidal zones, gypsum is deposited clastically, with microbial mats occupying the sediment to a depth of several centimeters. In these regions, mixed gypsum and organic nodule protrusions are elevated up to 5cm above the surface (Vogel 2009).

Buck Reef Chert

At the sampled facies, chert is banded black-and-white with a thickness of up to 15 cm for the black layers and 10 cm for the white. White bands are composed of nearly pure microcrystalline quartz, but occasionally host anastomosing dark carbonaceous laminations. Black bands show a relatively complex internal structure including rounded and sand-sized detrital silica and carbonaceous grains, small quantities of siderite, and irregular carbonaceous matter. The carbonaceous matter in this facies demonstrates a significant differential in the time of silicification, with breccia trapping white chert fragments in black layers of considerable plasticity. Most provocatively, black bands show thin carbonaceous laminations that form a dense web around large silica grains, sometimes draping over surface deformations. These laminations contain long carbonaceous filaments on the micrometer scale. Deformities and brecciation in the black bands gradually fade at higher in the stratigraphic succession, with little evidence of filamentous carbon deposits or surface deformation; rounded detrital particles give

way to irregular grains with a wider range of densities and carbonaceous laminations adhere closely to underlying particles where they exist at all.

Rounded silica and preferentially sand-sized grains imply sorting in an aqueous environment. Coupled with the wide extent and low density of the deposits, this suggests a shallow ocean shelf (15-200 m depth) influenced by wave action and some currents. Higher in the unit, finer deposits and less pronounced soft-sediment deformation indicate a progressively deepening depositional environment. The high plasticity and brecciation in the black carbonaceous bands implies meaningful resistance to tensile and shear stresses uncommon for sedimentary deposits. Tensile strength in these carbon-rich deposits is further implied by their tendency to trap or drape over grains. This resistance to shear stresses, in addition to structures composed of fine filaments and a marked scarcity within the aphotic zone, leads to the conclusion that these bands contain fossil remnants of bacterial mats dating to ~3.4 Ga (Tice & Lowe, 2004). A shallow ocean shelf would have allowed light to reach a bottom layer of sediment that was occupied by microbial colonies and was stirred and ripped by periodic storms. The microbes would form coherent mats over the sediment using a variety of extracellular proteins or colonial structures. As the overlying water column deepened, microbial arrangements showed a macroscopic response to low rates of sediment deposition and a scarcity of light, before the paucity of photosynthetically active radiation stymied growth completely.

CHAPTER II

SUMMARY OF INVESTIGATION

Introduction

Paleoarchean sedimentary rocks provide a morphological record of the earliest life on Earth (e.g., Hofmann et al., 1999; Walsh and Lowe, 1999; Westall et al., 2001; Tice and Lowe, 2004, 2006; Allwood et al., 2006; Schopf, 2006; Hofmann and Bolhar, 2007; Sugitani, 2007, 2009, 2010; Tice et al., 2011). However, with the notable exception of the Strelley Pool Chert stromatolite reef (Allwood et al., 2006), nearly all known examples of Paleoarchean microfossils and fossilized microbial communities are discontinuous and limited in both lateral and vertical extent. It is not clear if this limitation results from poor preservation or a fundamentally weakly developed Paleoarchean biosphere.

In particular, the 3.42 Ga Buck Reef Chert (Kromberg Formation, Barberton greenstone belt, South Africa) contains evidence of benthic microbial communities preserved in black-and-white banded cherts deposited on a storm-influenced platform (Tice & Lowe, 2004, 2006a, 2006b; Hofmann and Bolhar, 2007; Tice 2009). Black bands in the platform facies contain abundant carbonaceous matter in the form of abundant detrital grains and rare fossil mats. Mats are thin, frequently partially eroded, rarely occur in successive bands, and visible only in thin section. The paucity of preserved communities has inhibited studies of microbial community interactions, responses to environmental perturbations, and relationships to sedimentation.

Recent investigations find evidence that the physical deposition of silica grains may have contributed to the formation of translucent white bands in black-and-white banded chert, in contrast to previous interpretations of diagenetic chemical precipitation (Stefurak et. al., 2014). This structural observation expands the scope of potential biogenic contributions to Paleoarchean chert beds. Pursuant to this line of inquiry, I investigate samples collected from the platform facies of the Buck Reef Chert by etching with hydrofluoric acid (HF) vapor and by cutting slabs thin enough to be transparent to light in order to visualize distributions of opaque material in black and white bands, respectively. These methods greatly expand the mesoscale

Methods

Cut rock slabs were etched with HF vapor by modifying existing methods for thin section etching (Westall, 2001). On the flat surface of a chert slab, HF reactions are more energetically favorable in regions of pure silica. Wherever carbonaceous features have been preserved by the surrounding matrix, this etching reaction is less pronounced. During a brief exposure to HF aerosol, therefore, extensive carbonaceous structures can be characterized, distinct from regions dominated by detrital accumulation or microquartz precipitation. This process simulates weathering of rocks in outcrop but can be controlled to result in spatially uniform weathering depth across multiple layers, avoids overgrowth by lichen, and thus optimizes visualization of carbonaceous features.

Twenty-five samples previously gathered from the BRC were prepared for analysis by cutting standard cm-thickness slabs on a diamond edged abrasive rock saw. Slab thickness ranged from 4-24 cm, with a representative sampling of black and white chert banding. Two adjacent slabs from each sample were taken, with facing surfaces polished using 600-grade carbide powder.

A 14 L Nalgene dessicator was used as a vacuum chamber. 1 mL of 48% HF liquid solution was added to the base of the dessicator. The sample slab was placed on an elevated platform with the facing side exposed to air/vacuum. The desiccator was sealed and air was evacuated from the chamber. The sample was exposed to aerosolized HF for a period of 3-12 hours (dependent on sample size, determined by visual inspection). After etching was visible, the slab was rinsed with 2 L nanopure water and air dried.

Unpolished facing slabs were cut to 3-5 mm thickness on a rock saw. Areas of pure chert were translucent at this thickness when brightly illuminated with transmitted light, allowing visualization of trace impurities. Opaque material grains and laminations were identified by Raman microspectroscopy. High-resolution photographs were taken of each etched sample, and each thin slab on a standard light table. White band layers in thin slabs were classified electronically by ImageJ software according to the number of relative opacity maxima in each band, for variations >2 mm.

Figure 1: A) Standard slab. B) Etched slab, with variations in sediment fabric across black bands. C) Thin slab, 2 mm thickness. Local maxima in lamination thickness are visible throughout white bands, and are conformable across breaks. D) White band laminatio

Results

In thin slabs, dark, densely packed laterally continuous anastomosing laminations identical to the anastomosing or β-type mats of Tice (2009) are visible throughout all white bands (Fig. 1). These laminations vary in frequency with stratigraphic depth, ranging from 30-90% of total volume. Within each band, lamination density varies cyclically, with regions of low density between local maxima that define distinct layers within white bands. These layers are not constant in thickness or frequency per band. Detrital grains are infrequent and typically enclosed within eyelets defined by underlying and overlying carbonaceous laminations (Fig. 1D). Some mat-like structures are present in the black bands of thin slabs and thin sections. These structures occupy <5% of total volume in black bands consistent with existing observations (Tice, 2009), and none are laterally continuous across the width of a hand sample.

Raman spectrographic analysis shows that thickly laminated regions have elevated peaks at both D and O wavenumbers (1330 cm^{-1} and 1600 cm^{-1}) (Figure 3). The O peak is produced by interactions with ordered planar graphite, with a shoulder extending to the 1610 range suggesting that some graphite is polycrystalline. The D peak, with higher amplitude than the O peak in most measured samples, indicates interactions with disordered carbonaceous matter. Together, these results are strongly consistent with the presence of mature greenschist carbonaceous inclusions, which were therefore primary to the rock (Figure 2). These results are similar to measured values in

black bands, previously interpreted as detrital carbonaceous grains and thickly laminated microbial mats.

Wide variations in HF-etched slabs are visible, further differentiating between black, white, and quartz-fill microfacies that were homogeneous prior to etching. Grain shape varies from high sphericity to low sphericity within black bands, consistent with variable rates of compaction. Grains are well rounded, with occasional microbial mat features. These are limited to the cm scale in lateral extent. We observe eroded mat fragments in the black banding consistent with destructive long-distance transport. Both grains and ripped mat fragments are vertically distributed according to hydraulic sorting (either according to their own properties or, when mats are attached to grain surfaces, the aggregate properties of the clumped lithology). Laminations in black bands are rare, and not graded.

In most cases, white bands remain undifferentiated after etching. Rarely, etching produced visible laminations in white bands, typically near their tops.

Thin sections confirm the relative frequency of mat-like laminations and detrital carbonaceous grains in each facies. Extensive anastomosing laminations appear in white bands, and less frequently in black band facies. Eyelet structures appear in both, typically on the 100-500 μm scale. No roll-up structures were found in white bands, in contrast with previous studies of black bands in thin section. Detrital grains form a very small (<2%) fraction of white bands relative to overall sedimentation. Sudden breakage of this layer can occur; anastomosing

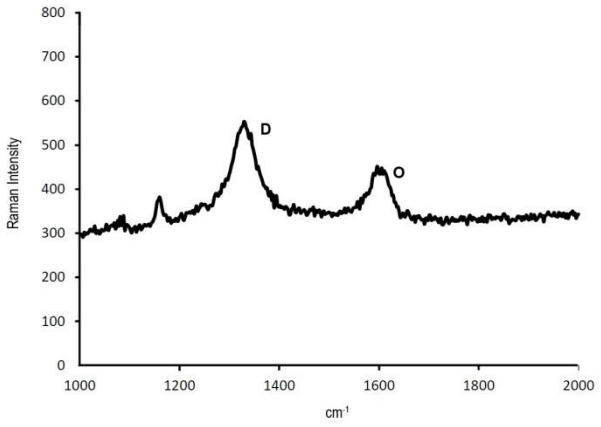

Figure 2: Sample Raman Spectroscopy of thickly laminated white bands in thin slabs. Peaks represent interaction with ordered planar graphite and disordered disordered carbonaceous matter.

laminations terminate against vertical breaks rather than approaching them asymptotically.

Interpretation

These observations are inconsistent with a purely detrital or inorganic chemical depositional system. Raman spectroscopy confirms that laminations are primary carbon-rich deposits. Eyelet structures demonstrate that laminations possessed tensile strength before burial and lithification. Throughout white bands (Figure 1D), laminations are distorted past the width of the grain itself at these locations, showing the lateral transmission of force through beds at the time of deposition. Furthermore, this distortion occurs in laminations above as well as below the grain, demonstrating that these

distortions are related to topological features and not impact force alone. Typically, eyelets are interpreted as draping behavior in microbial mat EPS during and immediately after grain --capture events. Filamentous laminations in both black and white layers are of a uniform thickness of ~30 micrometers, in contrast to white and black band variability; compaction alone is unlikely to produce this uniformity. It is therefore unlikely that laminations represent a compressed layer of detrital carbonaceous sediments. We conclude that these laminations record the growth of microbial mats in beds previously thought to be inorganic chemical precipitates. These laminations contribute fully 30-90% of rock volume in white bands, suggesting that microbial biomass dominated the ancient Buck Reef Chert geologic platform.

Recent investigations raise the possibility that detrital silica granules contribute to white band formation, producing the anastomosing features in part through the later compaction of detrital sediments within a darker matrix (Stefurak et. al., 2014). While detrital silica accumulation is fully consistent with our proposed growth model, the lenticular silica gaps between anastomosing mat laminations are unlikely to be the product of compaction. A measurement of isolated carbonaceous grains trapped in the white band biofilm shows that these darker grains typically have low aspect ratios; compaction in sampled white bands was minimal.

The high detrital fraction in black bands suggests that sedimentary conditions were not favorable to biomat accumulation, likely a product of rapid sediment accumulation. Many mat structures within black bands show signs of ripping and transport. However, others show draping behavior over eyelets, implying that they grew

on stable surfaces within black bands and were later buried; black bands may represent multiple clustered detrital events, rather than a single energetic phase of deposition. Notably, these biofilms show the same 30 μm thickness as mats in the microbially dominated white bands.

Within white bands, cyclicity in mat density may provide additional information pertaining to growth patterns in the microbial ecosystem. Distance between regions of maximum density is highly variable, ranging from 1 cm to 4 cm in observed samples. Several distinct local maxima may exist within individual white bands (Figure 1).. The number of isolated layers per band may be compared to standard probability distributions using Monte Carlo methods. Since a particular hypothesis concerning mat growth patterns will correspond to a specific probability distribution, we can use this statistical method to consider certain depositional models.

A simple interpretation of mat cyclicity is that measured peaks represent seasonal variations in growth rate, with biomass tending to dominate the facies during periods of rapid growth and chemical precipitation increasing as a fraction when seasonal limitations inhibit biological metabolism. In this model, black bands are deposited by storm events or turbidity currents that recur at random with a fixed probability and white bands represent regular fluctuations in background conditions. As such, biomass peaks in white bands could be used as a measure of fixed time intervals between major depositional events. This model corresponds to the geometric distribution (Figure 3),

$$P(X=k) = (1-p)^{k-1}p$$

where k is the number of local maxima and p is the probability of a depositional event occurring within the time interval represented by each peak. Note that $1/p$ is an empirical factor, the mean number of peaks in white bands (2.13).

Interestingly, despite a low sample size, we see that this model is outside the 95% confidence interval of Monte Carlo simulations. Thus, mat number distributions show no evidence of Paleoarchean seasonal growth patterns.

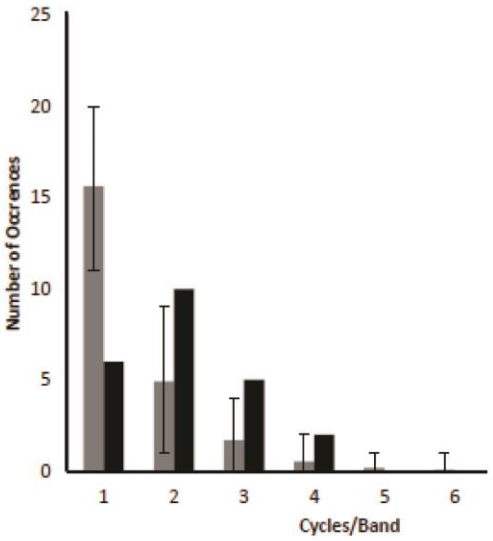

Figure 3: Measured values of mat peaks compared to a monte carlo simulation under geometric conditions corresponding to regular seasonal variations in mat thickness. p=0.47

We may consider a second model of mat accumulation, in which layering in white bands is driven by fluctuations in the rate of silica sedimentation, potentially driven by changes in water column silica concentrations, water column mixing, or transport of mud-like siliceous sediment. Mat growth is disrupted by erosion and deposition of detrital material during regular current active intervals, potentially stormy seasons. With black bands measuring discrete time intervals and mat density peaks recording maxima in water column chemical fluctuations, measurements are expected to follow a zero-truncated Poisson distribution (Figure 4):

$$P(X=k \mid k>0) = \frac{\lambda^k}{(e^{\lambda}-1)k!}$$

where k is the number of measured local maxima, and λ is the empirically estimated 1.76.

Monte Carlo simulation of the Poisson distribution along white band samples is fully consistent with measured frequencies. As such, the relative density of mat thickness may be inversely proportional to the rate of silica sedimentation within fixed accumulation of biological accumulation and a variable rate of inorganic deposition.

Biofilms themselves grow to a constant thickness independent of microfacies. In modern environments, mat thickness is typically limited by the rate at which nutrients diffuse through the local environment and by the depth of light penetration through EPS and overlying photoreactive pigments (Costerton et. al., 1995). These mats reach a steady state in which photosynthetic bacteria at the top of the mat produce additional

biomass, and heterotrophic organisms in the darker interior consume and remineralize this organic matter (Visscher & Stolz, 2005). Constant biofilm thickness in the Buck Reef Chert implies that microbes in these locations had reached equivalent metabolic limits.

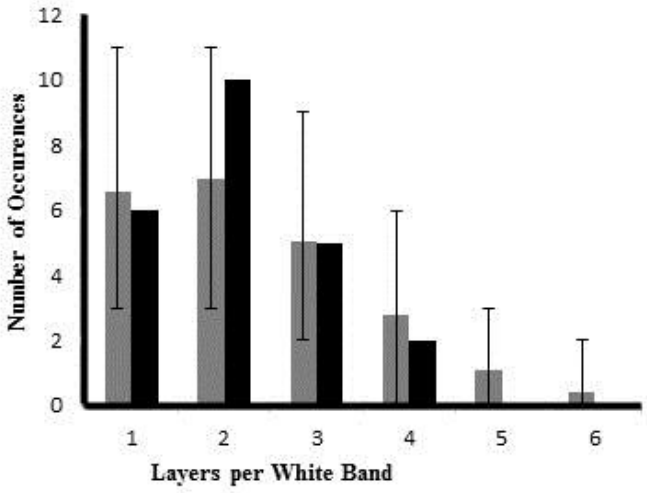

Figure 4: Intraband mat layers compared to zero-truncated Poisson distribution Monte Carlo simulation, corresponding to seasonal storm events and random fluctuations in silica sedimentation. λ=1.76

Sediments in the Buck Reef Chert accumulated at three distinct timescales. Biofilms reached typical thickness most quickly- in black bands, biofilm thickness remains constant even as mat density drops. The rate of silica sedimentation (both

detrital and chemical) varied on longer timescales within white bands. Although fossil biofilm thickness remains constant throughout these variations, the density of mats does not, corresponding to a greater supply of inorganic sediments. At the most broad scale, periods of high-energy deposition recur at intervals, with a radical but temporary impact for biogenic and detrital rates of sedimentation.

In conditions of primarily biological accumulation (minimal detrital or chemical sedimentation), biofilm thickness would grow to the characteristic 30 μm, and mat burial would be balanced by further growth- signified by higher mat density on lithification. Although mat structures fill a majority of white band volume, it may be that silica precipitation controlled the overall rate of sediment accumulation of these bands.

Dependencies between biomass accumulation and silica precipitation permit the preservation of microbial biofilms at rates not previously observed in the Buck Reef Chert. These fossil mats, found in every white band observed in this study, demonstrate that these geobiologically active ecosystems were ubiquitous on the 3.42 Ga platform.

REFERENCES

Allwood, A. C., et al. (2006). "Stromatolite reef from the Early Archaean era of Australia." Nature 441(7094): 714-718.

Allwood, A. C., et al. (2009). "Controls on development and diversity of Early Archean stromatolites." Proceedings of the National Academy of Sciences 106(24): 9548-9555.

Batchelor, M., et al. (2004). "A case for biotic morphogenesis of coniform stromatolites." Physica A: Statistical Mechanics and its Applications 337(1): 319-326.

Beukes, N. J. (1987). "Facies relations, depositional environments and diagenesis in a major early Proterozoic stromatolitic carbonate platform to basinal sequence, Campbellrand Subgroup, Transvaal Supergroup, southern Africa." Sedimentary Geology 54(1): 1-46.

Costerton, J. W., et al. (1995). "Microbial biofilms." Annual Review of Microbiology 49(1): 711-745.

Dupraz, C., et al. (2013). "Stromatolitic knobs in Storr's Lake (San Salvador, Bahamas): a model system for formation and alteration of laminae." Geobiology 11(6): 527-548.

Grotzinger, J. P. and A. H. Knoll (1999). "Stromatolites in Precambrian carbonates: Evolutionary mileposts or environmental dipsticks?" Annual Review of Earth and Planetary Sciences 27(1): 313-358.

Hofmann, H. J. (1973). "Stromatolites: Characteristics and utility." Earth-Science Reviews 9(4): 339-373.

Hofmann, A. and R. Bolhar (2007). "Carbonaceous cherts in the Barberton Greenstone Belt and their significance for the study of early life in the Archean record." Astrobiology 7(2): 355-388.

Hofmann, H. J. and G. D. Jackson (1987). "Proterozoic ministromatolites with radial-fibrous fabric." Sedimentology 34(6): 963-971.

Riding, R. (2011), “Microbialites, stromatolites, and thrombolites.” Encyclopedia of Geobiology, Springer: 635-654.

Schopf, J. W. (1993). "Microfossils of the Early Archean Apex Chert: New evidence of the antiquity of life." Science 260(5108): 640-646.

Simonson, B. M., et al. (1993). "Carbonate sedimentology of the early Precambrian Hamersley Group of western Australia." Precambrian Research 60(1): 287-335.

Stefurak, E. J. T., et al. (2014). "Primary silica granules—A new mode of Paleoarchean sedimentation." Geology 42(4): 283-286.

Stevens, G. and J.-F. Moyen (2007). "Metamorphism in the Barberton Granite Greenstone Terrain: a record of Paleoarchean accretion." Earth's Oldest Rocks. Developments in Precambrian Geology 15: 669-698.

Tice, M. M. (2009). "Environmental controls on photosynthetic microbial mat distribution and morphogenesis on a 3.42 Ga clastic-starved platform." Astrobiology 9(10): 989-1000.

Tice, M. M. and D. R. Lowe (2004). "Photosynthetic microbial mats in the 3,416-Myr-old ocean." Nature 431(7008): 549-552.

Tice, M. M., et al. (2011). "Archean microbial mat communities." Annual Review of Earth and Planetary Sciences 39: 297-319.

van Zuilen, M. A., et al. (2007). "Carbonaceous cherts of the Barberton Greenstone Belt, South Africa: Isotopic, chemical and structural characteristics of individual microstructures." Geochimica et Cosmochimica Acta 71(3): 655-669.

Visscher, P. T. and J. F. Stolz (2005). "Microbial mats as bioreactors: populations, processes, and products." Palaeogeography, Palaeoclimatology, Palaeoecology 219(1–2): 87-100.

Vogel, M. B., et al. (2009). "The role of biofilms in the sedimentology of actively forming gypsum deposits at Guerrero Negro, Mexico." Astrobiology 9(9): 875-893.

Westall, F., et al. (2001). "Early Archean fossil bacteria and biofilms in hydrothermally-influenced sediments from the Barberton greenstone belt, South Africa." Precambrian Research 106(1–2): 93-116.

APPENDIX A

HAND SAMPLE AND THIN SECTION DATA

Figure A1: Sample TSA5-45. A: Etched slab. B: Thin slab. (Thin section found in Figure 1D of Chapter II)

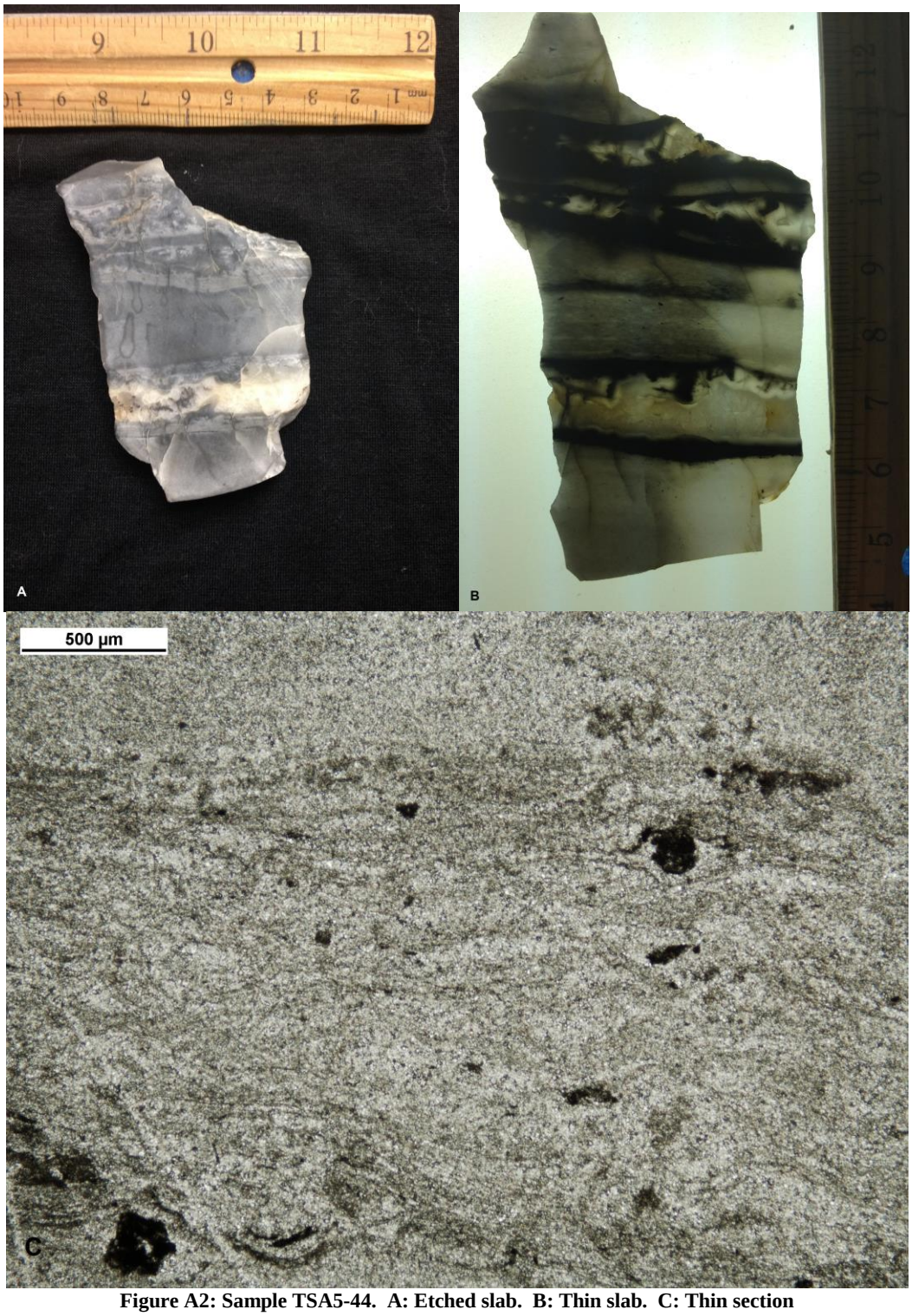

Figure A2: Sample TSA5-44. A: Etched slab. B: Thin slab. C: Thin section

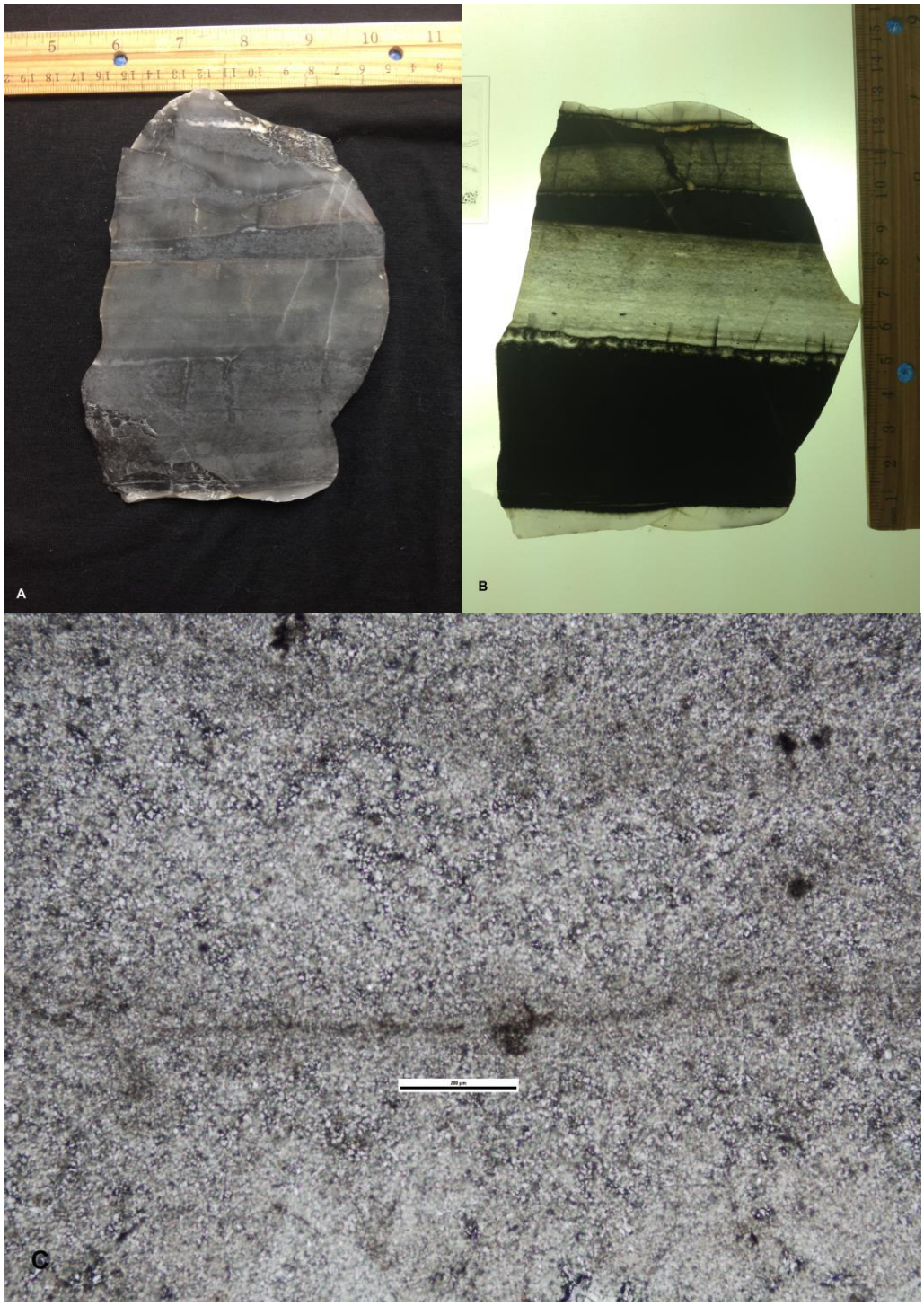

Figure A3: Sample TSA10-8-9. A: Etched slab. B: Thin slab. C: Thin section

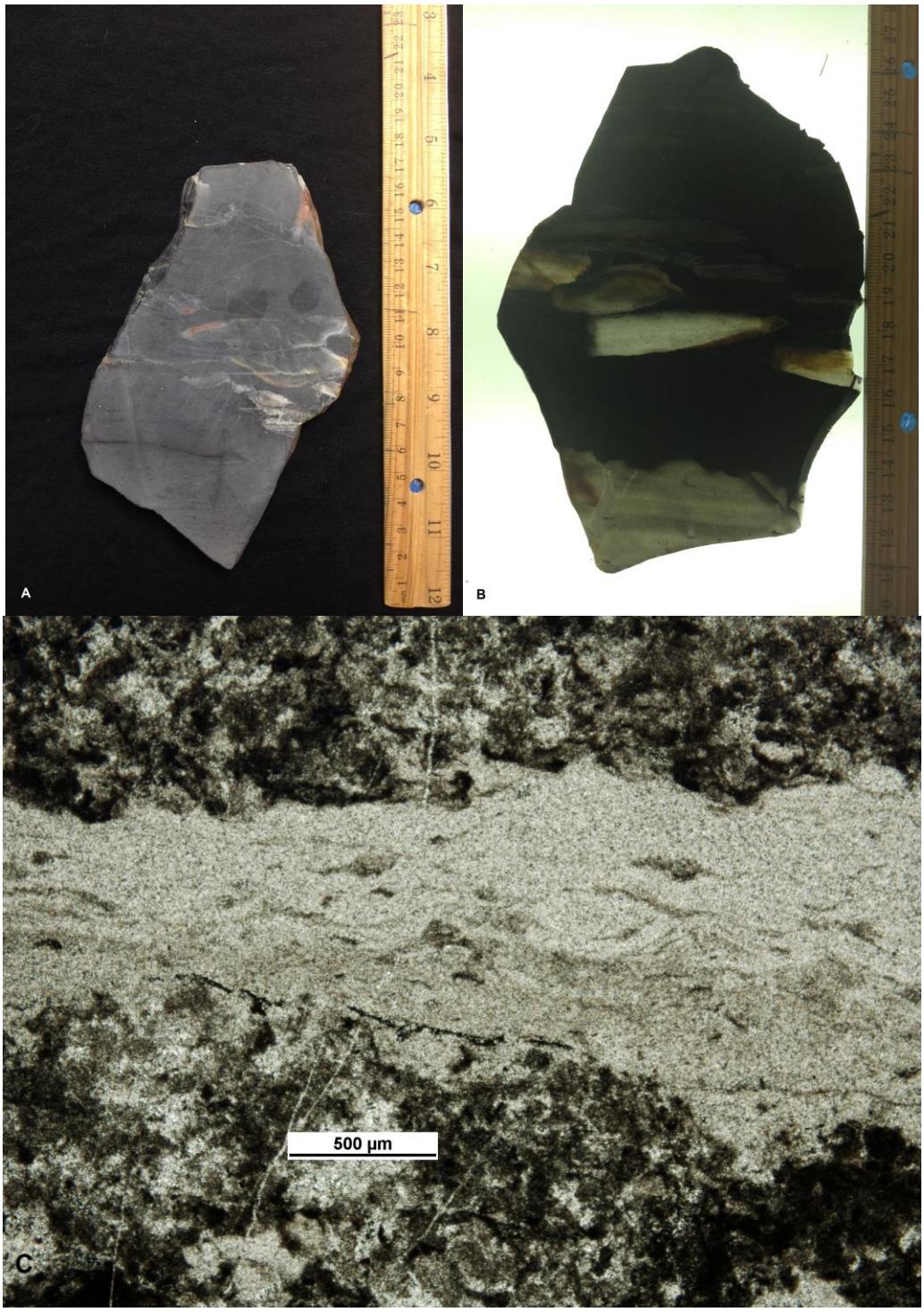

Figure A4: Sample TSA10-8-5. A: Etched slab. B: Thin slab. C: Thin section

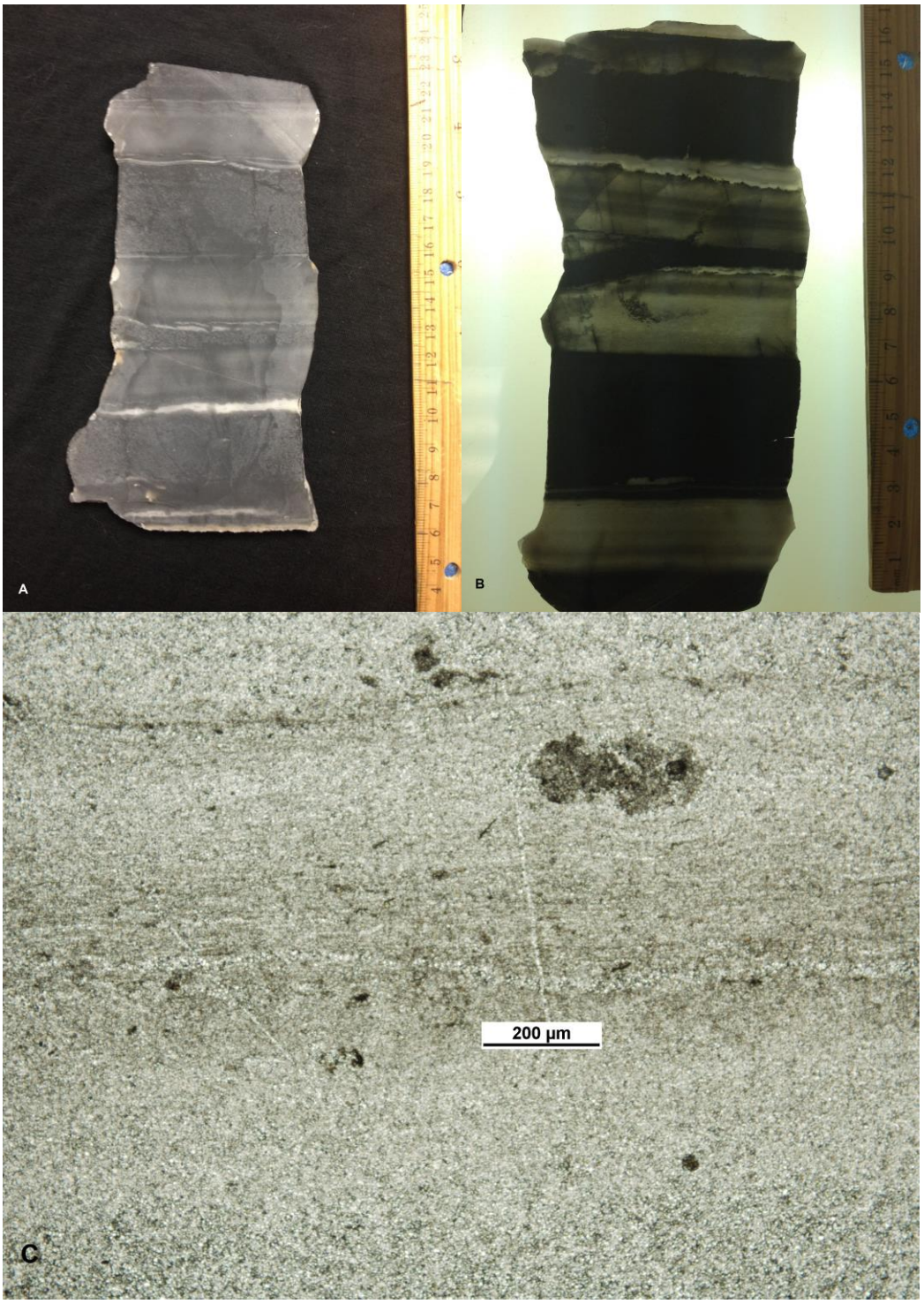

Figure A5: Sample TSA10-8-6. A: Etched slab. B: Thin slab. C: Thin section